Nature of intensity and phase modulations in stimulated Brillouin scattering

Shahraam Afshaarvahid,* Vladimyros Devrelis,† and Jesper Munch

Department of Physics and Mathematical Physics, The University of Adelaide, Adelaide, South Australia 5005, Australia
(Received 14 August 1997)

The nature of stimulated Brillouin scattering (SBS) temporal modulations for a focused beam in a finite-length cell with homogeneous medium is examined numerically. The finite phonon lifetime produces deterministic oscillations at the threshold while the inclusion of the random noise as an initiation source of SBS leads to stochastic fluctuations in Stokes intensity and phase. A unified study of both modulations under different parameters is presented. The results indicate a large useful parameter space for excellent Stokes beam quality. [S1050-2947(98)05405-5]

PACS number(s): 42.65.Es, 42.65.Hw

I. INTRODUCTION

The dynamics of stimulated Brillouin scattering (SBS) has been widely investigated because of its importance in optical phase conjugation [1,2], pulse compression [3,4], and beam combination [5–7]. SBS is a nonlinear process where energy is exchanged from the laser beam to the Stokes beam through an interaction with a sound wave. When used in an optical element, SBS is usually deployed either as an amplifier with an externally applied Stokes field, or as a SBS generator. The theory of SBS amplifiers is simpler than that of SBS generators since the Stokes field is externally applied, whereas the analysis of SBS generators requires the inclusion of the thermal density fluctuations of the medium as the source for the initiation of the process. This stochastic initiation of SBS leads to fluctuations in the Stokes field's amplitude and phase [1,8–12]. These fluctuations are important in practical applications since they reduce the coherence length of the scattered beam [13] and have been observed to reduce the temporal and spatial fidelity of the SBS process [14–17]. Early experimental observations of the presence of phase jumps and amplitude fluctuations in SBS were reported in 1980 [18–20]. More recent theoretical and experimental investigations of these fluctuations in optical fibers have been made by Dianov *et al.* [9], Gaeta and Boyd [11], and Kuzin *et al.* [21]. Their investigations showed that large scale fluctuations in the Stokes intensity occur when the transit time through the interaction region is much greater than the phonon lifetime. Intensity and phase fluctuations have been investigated experimentally also for short interaction lengths typical of a focused geometry [15,13,12,16]. Simultaneous fluctuations in the Stokes amplitude and beam quality have been observed [15] as has actual variation in the phase of the Stokes beam, measured directly by heterodyne detection [13]. In addition, the effect on these simultaneous fluctuations of experimental parameters such as the interaction length and input energy have been reported [12,16]. Numerical models have also shown simultaneous occurrence of jumps in the Stokes phase and fluctuations in the Stokes reflectivity and fidelity [8,14]. Similar fluctuations were also predicted [22,23] and observed [24,25] in stimulated Raman scattering and recognized as solitons.

Most published theoretical studies of SBS have dealt with SBS amplifiers or generators in the undepleted or steady state regime where the Stokes wave was either applied externally or initiated inside the medium from a constant or localized source. In this paper we present a single unified theoretical approach to SBS in a focused cell geometry, for the transient and depleted regimes while seeded from distributed random noise typical of most practical applications. We have developed a numerical model to examine in detail how the scattered Stokes beam is initiated from noise and propagated through the medium, and what parameters affect its amplitude and phase modulation. We use a Gaussian random noise distribution [9,11] (both in space and time) as a source for the SBS process in order to simulate the actual thermal fluctuations in the density of the medium.

Our model predicts two kinds of amplitude modulation: (a) deterministic relaxation oscillations at the threshold due to finite phonon lifetime and (b) stochastic fluctuations caused by the random noise source. An extensive examination of the behavior of the deterministic oscillations includes the following parameters: phonon lifetime, focal length, immersion length, and input energy, and it reveals under what parameter regimes these oscillations result in a pulse-compressed Stokes beam. This is followed by the study of stochastic fluctuations and their dependence on parameters such as phonon lifetime, immersion length, input energy, and pulse duration. Although many authors identify these fluctuations as being due to phase jumps, our model shows that phase and intensity fluctuations are coupled via the nonlinear interaction, and thus occur simultaneously, denying the existence of a causal relationship to the phenomenon. This was determined by tracing the fluctuations back to the time of initiation. The parameter regime required for achieving excellent beam quality (amplitude and phase fidelity) is evaluated.

II. THEORY

The equations describing the SBS process are derived from Maxwell's equations for the electric fields and Navier-Stokes equation for the acoustic field inside the material. Writing the electric and acoustic fields as [26]

*Electronic address: shahraam@physics.adelaide.edu.au
†Present address: DSTO, Salisbury SA 5108, Australia.

$$E_p = \frac{1}{2}[\Psi_p(z,t)e^{i(\omega_p t + k_p z)} + \Psi_p^*(z,t)e^{-i(\omega_p t + k_p z)}],$$

$$E_s = \frac{1}{2}[\Psi_s(z,t)e^{i(\omega_s t - k_s z)} + \Psi_s^*(z,t)e^{-i(\omega_s t - k_s z)}], \quad (1)$$

$$E_q = \frac{1}{2}[\Psi_q(z,t)e^{i(\omega_q t + k_q z)} + \Psi_q^*(z,t)e^{-i(\omega_q t + k_q z)}]$$

(where E_p, E_s, and E_q are the pump, Stokes, and acoustic fields, respectively), neglecting the transverse field variations, and using the slowly varying envelope approximation, the following coupled wave equations can be derived [27].

$$\left(\frac{\partial}{\partial z} - \frac{n}{c}\frac{\partial}{\partial t}\right)\Psi_p = ig_1\Psi_q\Psi_s,$$

$$\left(\frac{\partial}{\partial z} + \frac{n}{c}\frac{\partial}{\partial t}\right)\Psi_s = -ig_1\Psi_q^*\Psi_p, \quad (2)$$

$$\left(\frac{\partial}{\partial t} + \Gamma\right)\Psi_q = -ig_2\Psi_p\Psi_s^*.$$

Here g_1 and g_2 are coupling coefficients, Γ is the damping rate (i.e., $\Gamma = 1/2\tau$ where τ is the phonon lifetime of the medium), and n is the refractive index of the medium.

In order to find the equations for the amplitudes and the phases of the fields we write the complex amplitudes Ψ_μ (where $\mu = p,s,q$) as

$$\Psi_\mu = A_\mu e^{-i\phi_\mu},$$

where A_μ and ϕ_μ are real functions. Substituting the new definition into the above equations results in a set of six coupled differential equations:

$$\left(\frac{\partial}{\partial z} - \frac{n}{c}\frac{\partial}{\partial t}\right)A_p = -g_1\sin(\phi_p - \phi_s - \phi_q)A_qA_s, \quad (3a)$$

$$\left(\frac{\partial}{\partial z} + \frac{n}{c}\frac{\partial}{\partial t}\right)A_s = g_1\sin(\phi_s + \phi_q - \phi_p)A_qA_p, \quad (3b)$$

$$\left(\frac{\partial}{\partial t} + \Gamma\right)A_q = g_2\sin(\phi_s + \phi_q - \phi_p)A_sA_p + f_1, \quad (3c)$$

$$\left(\frac{\partial}{\partial z} - \frac{n}{c}\frac{\partial}{\partial t}\right)\phi_p = -g_1\cos(\phi_p - \phi_s - \phi_q)\frac{A_qA_s}{A_p}, \quad (3d)$$

$$\left(\frac{\partial}{\partial z} + \frac{n}{c}\frac{\partial}{\partial t}\right)\phi_s = g_1\cos(\phi_s + \phi_q - \phi_p)\frac{A_qA_p}{A_s}, \quad (3e)$$

$$\left(\frac{\partial}{\partial t}\right)\phi_q = g_2\cos(\phi_s + \phi_q - \phi_p)\frac{A_sA_p}{A_q} + f_2. \quad (3f)$$

To represent the noise initiation of the SBS process, we have added two Langevin forces f_1 and f_2, with spatial and temporal Gaussian distributions [11]. Both f_1 and f_2 are δ correlated functions in the sense that

$$\langle f_i(z,t)f_i^*(z',t')\rangle = Q\delta(z-z')\delta(t-t'),$$

where Q is given by [10]

$$Q = \frac{2kT\rho_0\Gamma}{v^2A}.$$

Here k is the Boltzmann constant, T is the temperature, ρ_0 is mean density, v is the velocity of sound in the material, and A is the cross sectional area of the interaction region.

For the phase-locked condition [i.e., $\sin(\phi_s + \phi_q - \phi_p) = 1$] and the steady state regime of SBS [i.e., ignoring all $(\partial/\partial t)A_\mu$], Eq. (3b) can be written as

$$\frac{\partial}{\partial z}A_s = \frac{g_1g_2}{\Gamma}A_p^2A_s, \quad (4)$$

which has a solution of $A_s = A_{s0}\exp[(g_1g_2/\Gamma)A_p^2l_{imm}]$ valid near threshold and without pump depletion. This leads directly to the usual expression for the steady state gain, given by $G = gI_pl_{imm}$, where I_p is the input pump intensity, l_{imm} is the active medium immersion length, and $g = g_1g_2\Gamma^{-1}$.

Some authors (e.g., [28,29]) have used the phase-locked condition for which SBS has the highest gain, i.e., $\phi_p - \phi_s - \phi_q = \pi/2$. When SBS starts from noise, a random noise distribution of $\phi_p - \phi_s - \phi_q$ is initially present. But as the phase-locked waves (those with $\phi_p - \phi_s - \phi_q = \pi/2$) have the highest gain in the medium, they suppress other Stokes waves with unlocked phases. By applying this condition to Eqs. (3), they are simplified to a set of three real coupled equations for the amplitudes. However, in order to explain the experimental observation of the simultaneous occurrence of intensity fluctuations and phase jumps [13], we have retained the complex equations since this is the only way that the phase of the Stokes field can be coupled to its intensity.

Equations (3) are nonlinear due to the terms $\sin(\phi_s + \phi_q - \phi_p)$ or $\cos(\phi_p - \phi_s - \phi_q)$. Although the behavior of the fields and their phases is seen better by these equations, and we use them whenever we want to provide a qualitative explanation, solutions of the equations require that we rewrite them for the real and imaginary parts of the fields. Using

$$\Psi_\mu = W_\mu + iV_\mu,$$

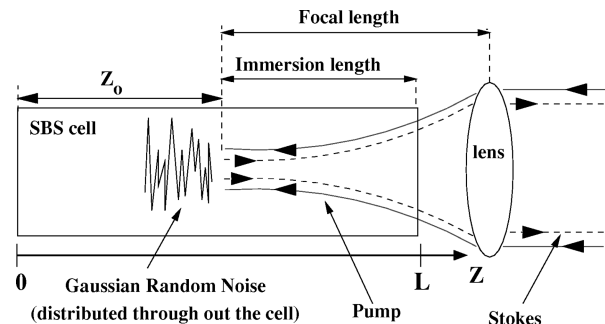the equations for the real and imaginary parts of the fields are

FIG. 1. The geometry used for the SBS process.

$$\left(\frac{\partial}{\partial z}-\frac{n}{c}\frac{\partial}{\partial t}\right)W_p=-g_1(W_qV_s+V_qW_s),$$

$$\left(\frac{\partial}{\partial z}+\frac{n}{c}\frac{\partial}{\partial t}\right)W_s=g_1(W_qV_p-V_qW_p),$$

$$\left(\frac{\partial}{\partial t}+\Gamma\right)W_q=-g_2(W_pV_s-V_pW_s)+f_1,$$

$$(5)$$

$$\left(\frac{\partial}{\partial z}-\frac{n}{c}\frac{\partial}{\partial t}\right)V_p=g_1(W_qW_s-V_qV_s),$$

$$\left(\frac{\partial}{\partial z}+\frac{n}{c}\frac{\partial}{\partial t}\right)V_s=g_1(W_qW_p+V_qV_p),$$

$$\left(\frac{\partial}{\partial t}+\Gamma\right)V_q=-g_2(W_pW_s/V_pV_s)+f_2.$$

The focusing geometry required for simulation of experiments is introduced using an approach similar to that of Menzel and Eichler [30]. Although SBS is primarily used to compensate for optical aberrations, we have chosen not to include spatial aberrations in this treatment, but concentrate entirely on temporal fluctuations or ''temporal fidelity'' of the Stokes beam. This is important, because lack of temporal fidelity leads to degradation of the Stokes return and hence a reduction in average reflectivity and efficiency of a phase conjugated laser system [14–16]. We are thus using spatially unaberrated Gaussian beams for both pump and Stokes fields, and we have made the further approximation that both these fields have the same Gaussian beam parameters (see Fig. 1):

$$\omega^2(z)=\omega_0^2\left[1+\left(\frac{(z-z_0)\lambda}{\pi\omega_0^2 n}\right)^2\right],$$

where ω_0 is the radius at the waist of the beam, λ is the wavelength, and n is the appropriate index of refraction as a function of z. This is a reasonable approximation in an efficient phase conjugating system where the fields are well above threshold and is justified by experimental results showing that the beam quality and divergence of the Stokes beam are indistinguishable from those of the pump beam when well above threshold. For an unaberrated beam this is only an approximation but is justified in our case where we concentrate on the temporal fidelity only.

As a result, the pump and Stokes intensities, $I_p=W_p^2+V_p^2$ or $I_s=W_s^2+V_s^2$, are changing not only because of the nonlinear interaction with the material but also because of the change in area of the beams. Keeping in mind that for a Gaussian beam the electric field amplitude has $\omega(z)$ in the denominator, we add $-[W_\nu/\omega(z)](\partial/\partial z)\omega(z)$ or $-[V_\nu/\omega(z)](\partial/\partial z)\omega(z)$ to the right hand side of equations for W_ν or V_ν ($\nu=p$ or s) to represent the change in the intensity due to focusing geometry [30]. Defining

$$\Psi_\nu=\frac{\Psi'_\nu}{\omega(z)}=\frac{W'_\nu}{\omega(z)}+i\frac{V'_\nu}{\omega(z)},$$

$$\Psi'_\nu=W'_\nu+iV'_\nu,$$

and hence,

$$W_\nu=\frac{W'_\nu}{\omega(z)},$$

$$V_\nu=\frac{V'_\nu}{\omega(z)},$$

it can be easily seen that $|\Psi'_\nu|^2=|\Psi_\nu|^2\omega^2(z)$ is the local power of the pump or the Stokes fields. Adding $-[W_\nu/\omega(z)](\partial/\partial z)\omega(z)$ or $-[V_\nu/\omega(z)](\partial/\partial z)\omega(z)$ to the right hand side of equations for W_ν or V_ν [i.e., Eqs. (5)] and rewriting these equations for prime fields, we find

$$\left(\frac{\partial}{\partial z}-\frac{n}{c}\frac{\partial}{\partial t}\right)W'_p=-g_1(W_qV'_s+V_qW'_s),\qquad(6a)$$

$$\left(\frac{\partial}{\partial z}+\frac{n}{c}\frac{\partial}{\partial t}\right)W'_s=g_1(W_qV'_p-V_qW'_p),\qquad(6b)$$

$$\left(\frac{\partial}{\partial t}+\Gamma\right)W_q=-\frac{g_2}{\omega^2(z)}(W'_pV'_s-V'_pW'_s)+f_1,\qquad(6c)$$

$$\left(\frac{\partial}{\partial z}-\frac{n}{c}\frac{\partial}{\partial t}\right)V'_p=g_1(W_qW'_s-V_qV'_s),\qquad(6d)$$

$$\left(\frac{\partial}{\partial z}+\frac{n}{c}\frac{\partial}{\partial t}\right)V'_s=-g_1(W_qW'_p+V_qV'_p),\qquad(6e)$$

$$\left(\frac{\partial}{\partial t}+\Gamma\right)V_q=-\frac{g_2}{\omega^2(z)}(W'_pW'_s+V'_pV'_s)+f_2.\qquad(6f)$$

We see that the new equations have a form similar to Eqs. (5). The only difference is that the prime fields are the power components instead of intensity components in Eqs. (5). The same procedure can be done for Eqs. (3) to get the following equations for the Stokes, pump, and acoustic grating power:

$$\left(\frac{\partial}{\partial z}-\frac{n}{c}\frac{\partial}{\partial t}\right)A'_p=-g_1\sin(\phi_p-\phi_s-\phi_q)A_qA'_s,\quad(7a)$$

$$\left(\frac{\partial}{\partial z}+\frac{n}{c}\frac{\partial}{\partial t}\right)A'_s=g_1\sin(\phi_s+\phi_q-\phi_p)A_qA'_p,\quad(7b)$$

$$\left(\frac{\partial}{\partial t}+\Gamma\right)A_q=g_2\sin(\phi_s+\phi_q-\phi_p)\frac{A'_sA'_p}{\omega^2(z)}+f_1.\quad(7c)$$

The equation for the acoustic field shows how the amplitude of the field depends on the intensity of the Stokes and pump waves, implying a high acoustic field at high intensities of the pump and the Stokes fields.

Integrating the phonon fields [Eqs. (6c) and (6f)] and substituting in the rest of Eqs. (6), reduces the set of equations

(6a)–(6f) to four coupled differential equations for the field amplitude. The numerical analysis starts with these four equations. An efficient noniterative algorithm is used in which Simpson's rule is applied to approximate the phonon's integral and an implicit finite differencing in time and backward differencing scheme in space are used to write the equations for discrete field amplitudes W_{pj}^m, V_{pj}^m, W_{sj}^m, and V_{sj}^m, where $m=0,1,2,\ldots,M$ are time indices ($t=m\Delta t$) and $j=0,1,2,\ldots,n+1$ are space indices ($z=j\Delta z$) [29]. Field vectors at the time $(m+1)\Delta t$ are defined as

$$\vec{W}_p^{\,m+1}=\begin{pmatrix} W_{p1} \\ W_{p2} \\ \cdot \\ \cdot \\ \cdot \\ W_{pn} \end{pmatrix}^{m+1} , \quad \vec{V}_p^{\,m+1}=\begin{pmatrix} V_{p1} \\ V_{p2} \\ \cdot \\ \cdot \\ \cdot \\ V_{pn} \end{pmatrix}^{m+1} ,$$

$$\vec{W}_s^{\,m+1}=\begin{pmatrix} W_{s2} \\ W_{s3} \\ \cdot \\ \cdot \\ \cdot \\ W_{sn+1} \end{pmatrix}^{m+1} , \quad \vec{V}_s^{\,m+1}=\begin{pmatrix} V_{s2} \\ V_{s3} \\ \cdot \\ \cdot \\ \cdot \\ V_{sn+1} \end{pmatrix}^{m+1} ,$$

where $n+1$ is the total number of discrete points in space and W_{pn+1}, V_{pn+1}, W_{s1}, and V_{s1} are the initial values at boundaries.

Using the linearization scheme defined by Chu *et al.* [29], we obtain the final form of the set of algebraic equations for the vector fields as

$$A^m\vec{W}_p^{m+1}+C^m\vec{W}_s^{m+1}+D^m\vec{V}_s^{m+1}=\vec{V},$$

$$E^m\vec{W}_s^{m+1}+F^m\vec{W}_p^{m+1}+G^m\vec{V}_p^{m+1}=\vec{U}, \quad\quad (8)$$

$$A^m\vec{V}_p^{m+1}-D^m\vec{W}_s^{m+1}+C^m\vec{V}_s^{m+1}=\vec{W},$$

$$E^m\vec{V}_s^{m+1}-G^m\vec{W}_p^{m+1}+F^m\vec{V}_p^{m+1}=\vec{Z}.$$

Here, A^m, C^m, E^m, F^m, D^m, and G^m are $n\times n$ upper or lower tridiagonal matrices evaluated at time $m\Delta t$ and $\vec{V}$, $\vec{U}$, $\vec{W}$, and $\vec{Z}$ are $n\times 1$ vectors containing boundary conditions on the pump and Stokes at time $t=(m+1)\Delta t$. This set of equations can be solved numerically without the need for iteration. The matrix coefficients and vectors $\vec{V}$, $\vec{U}$, $\vec{W}$, and $\vec{Z}$ are evaluated recursively using the initial values of the Stokes and pump fields at $t=0$. Here the field amplitudes at any time slot $m+1$ have been determined from those at the preceding time slot m. To justify the validity of the linearization assumption, we used the field amplitudes at time slot $m+1$ to reevaluate iteratively the nonlinear coefficient involved in the differential equations. An improvement of only 4% was achieved after five iterations.

Solutions of Eqs. (8) are found for a Gaussian pump pulse of the form $E_0\exp\{-2[(t-t_0)/t_p]^2\}$, where t_p is the pulse
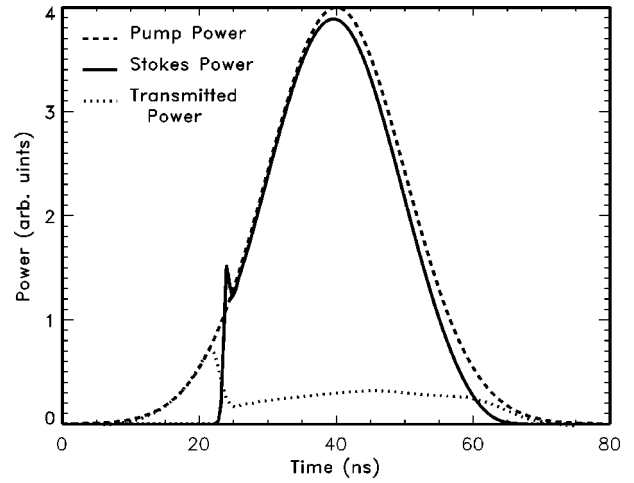

FIG. 2. Typical results for the Stokes, pump, and transmitted pulse.

width. Referring to Fig. 1, we apply the following geometrical and material parameters to examine the typical results of the SBS process: cell length 60 cm, focal length 50 cm, immersion length 15 cm, initial waist of the beam 0.4 cm, gain of the medium 0.0063 cm/MW, input energy 320 mJ, full width at half maximum (FWHM) pulse length 20 ns, phonon lifetime 0.85 ns, and index of refraction, $n=1.0$, with results shown in Fig. 2.

III. RESULTS AND DISCUSSION

Depending on the geometry of the SBS process and the energy of the input pulse, our model results in Stokes oscillations or fluctuations similar to those observed experimentally [18–20,15–17]. The intensity modulation can be categorized into two groups: (a) deterministic amplitude oscillations at the time when the energy of the pump reaches the threshold energy and (b) stochastic fluctuations due to noise in amplitude and phase of the Stokes beam.

A. Deterministic threshold oscillation

The finite phonon lifetime provides an energy interchange mechanism between the Stokes and laser field via the acoustic field. In the case of Gaussian pump beams, it takes some time for the energy contained in the pump to reach the threshold energy for Stokes initiation. At the threshold, the Stokes power increases very rapidly and overshoots the pump power, resulting in the depletion of the pump field and reduction of gain. Because of this gain reduction the Stokes power drops, causing an increase in the pump energy which in turn causes an increase in the Stokes field again. This energy interchange between the Stokes and pump fields continues and resembles a relaxation oscillation (see Fig. 3). The rate of this energy interchange is controlled by the reaction time of the acoustic field, i.e., phonon lifetime. Such an energy interchange mechanism has also been discussed in Refs. [4] and [29]. Chu *et al.* [29] report relaxation oscillations which are visible in the transmitted pulse. However, our simulation results show that for a long cell and a geometry in which the laser beam has been focused deeply into the cell, relaxation oscillation should be visible in the Stokes return as shown in Fig. 3.
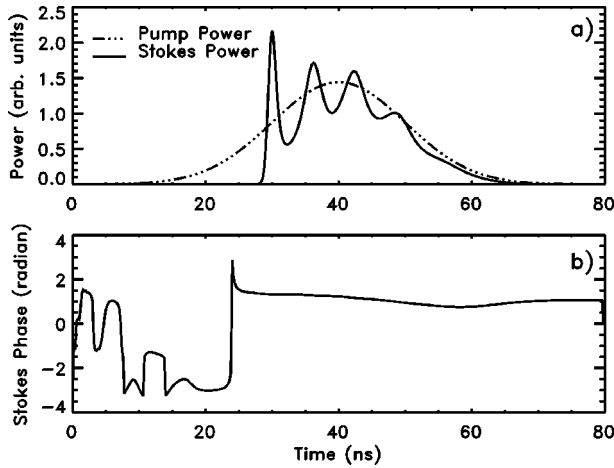
FIG. 3. (a) Typical threshold oscillation in the Stokes beam obtained for the following parameters: cell length 100 cm, focal length 100 cm, immersion length 70 cm, phonon lifetime 0.85 ns, medium gain 0.006 cm/MW, FWHM pulse length 20 ns, and input energy 114 mJ. (b) shows no corresponding variation in the phase of the Stokes.

In order to categorize the behavior of threshold oscillation we use the following parameters to run the simulation: Cell length 100 cm, focal length 100 cm, immersion length 70 cm, phonon lifetime 0.85 ns, gain of the medium 0.006 cm/ MW, FWHM pulse length 20 ns, and input energy 114 mJ. Any changes to these parameters are specified in the captions of the figures. Figure 3 shows a typical threshold oscillation in the Stokes beam. Different parameters such as phonon lifetime, laser intensity at the focal point, and immersion length affect the behavior of the threshold oscillation. There are no phase jumps predicted corresponding to these oscillations.

1. Effect of phonon lifetime on the threshold oscillation

If the finite phonon lifetime is responsible for the relaxation oscillation at the threshold energy, we would expect that the behavior of the threshold oscillations depends on this parameter. Figure 4 shows the threshold oscillation for two
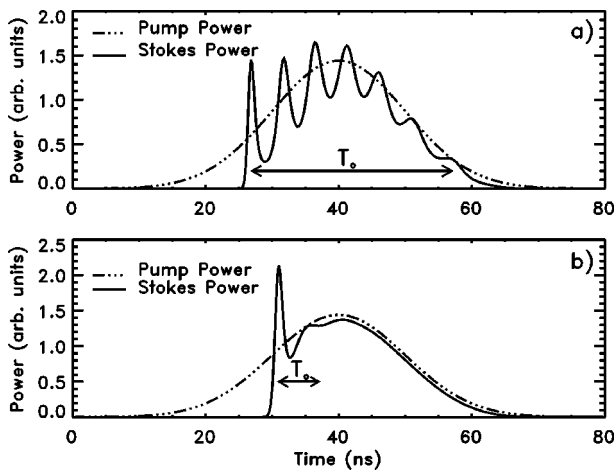

FIG. 4. Threshold oscillations are reduced for longer phonon lifetime. (a) Phonon lifetime is 0.5 ns and (b) phonon lifetime is 1.25 ns. Other parameters are as those of Fig. 3.
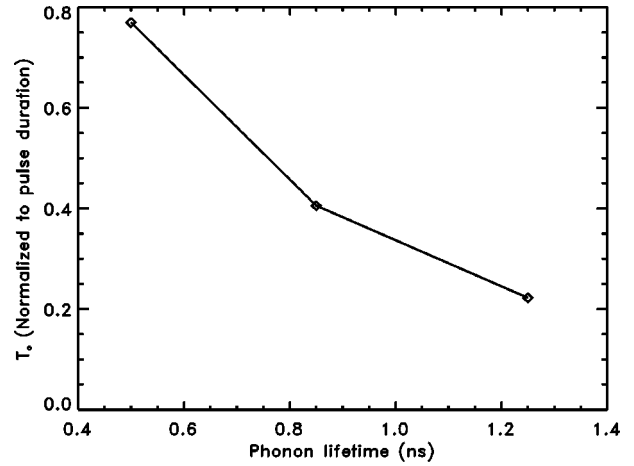

FIG. 5. A shorter relaxation oscillation is achieved for long phonon lifetime. The graph shows how T_0 (a time interval over which the oscillations are visible, see Fig. 4) is reduced for long phonon lifetime.

different phonon lifetimes. Defining T_0 to be the time interval over which the threshold oscillations are observable (see Fig. 4), our simulation predicts that T_0 is reduced for long phonon lifetime (see Fig. 5). It is seen that for longer phonon lifetimes, oscillations in the Stokes return come to an equilibrium faster than those for short phonon lifetimes. Our model permits a detailed investigation of the above mentioned relaxation oscillation and the role of the phonon lifetime.

The acoustic field is described by Eq. (3c). For early times in the process, the first source term in the right hand side of the equation may be ignored and for the second term we can write $f_1 = \Sigma_k a_k \sin \omega_k t$. Equation (3c) can then be solved as

$$\Psi_q = \Psi_{0q} e^{-\Gamma t} + \sum_k a'_k \sin \omega_k t + \sum_k b'_k \cos \omega_k t,$$

in which $a'_k = a_k \Gamma (\Gamma^2 + \omega_k^2)^{-1}$ and $b'_k = -a_k \omega_k (\Gamma^2 + \omega_k^2)^{-1}$. In the limit of a long phonon lifetime, i.e., $\Gamma \to 0 (\tau \to \infty)$, we find $a'_k = 0$ and $b'_k = -a_k/\omega_k$, which results in a solution of $\Psi_q = \Sigma_k - (a_k/\omega_k) \cos \omega_k t$ for the acoustic field. Comparing this result with the source term f_1, it is seen that in the limit of a large phonon lifetime the medium will not respond to the rapid fluctuations in the source term, but rather responds to the integral of rapid changes. In the other limit of $\Gamma \to \infty (\tau \to 0)$, $b'_k \to 0$ and $a'_k = a_k/\Gamma$ which gives a solution of $\Psi_q = \Sigma_k (a_k/\Gamma) \sin \omega_k t$. In this case the medium can cope with the rapid changes in the source term, thus resulting in a modulated Stokes pulse. The above discussion is applicable not only for the beginning of the process but also for any rapid changes in the source fields of the acoustic field. The phonon lifetime thus represents a measure of the inertia of the acoustic field. The larger the phonon lifetime, the higher is the inertia of the acoustic field and the slower is the response of the medium to the rapid changes in the Stokes and the laser field.

2. Effect of laser intensity at the focal plane

According to Eq. (7c), the amplitude of the acoustic field depends on the intensity of the input pulse. A shorter focal
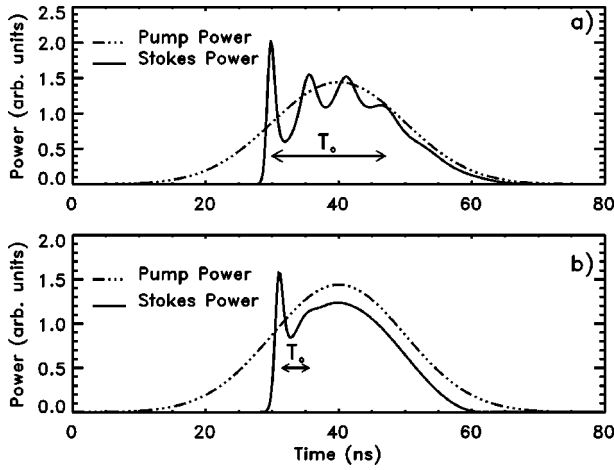
FIG. 6. Smaller focal spot (higher intensity) results in a suppression of threshold oscillations. Oscillations are reduced in (b) (focal length 60 cm) in comparison with (a) (focal length 90 cm). Other parameters as in Fig. 3.

length results in a higher intensity at the focal plane hence a higher power acoustic wave. As a result of this strong acoustic field, the Stokes amplitude does not reduce as quickly after overshooting, which in turn causes a shorter duration of the relaxation oscillation. This is illustrated in Fig. 6.

3. Effect of immersion length

Kuzin *et al.* [21] have discussed the influence of the depletion length (the length over which the laser pump beam experiences most of its depletion) on the suppression of fluctuations in the Stokes field. They emphasized that if the propagation time through the depletion length $T_{l_{dep}}$ is smaller than the temporal variation of the Stokes field at the beginning of the depletion region T_s, a smoothing of the Stokes field towards the output of the cell would take place. In this case we are in the steady state regime of SBS, and can rewrite Eqs. (3) in the phase-locked condition, as

$$\frac{\partial}{\partial z}I_p = 2gI_pI_s,$$

$$\frac{\partial}{\partial z}I_s = 2gI_pI_s. \tag{9}$$

Moving the origin of z to the entrance of the cell and writing $I_p(z) = I_s(z) + I_l$ [31] (where I_l is a constant indicating the degree of pump depletion), we can solve the differential equations (9) to find

$$I_s(z) = \frac{I_l I_s(0)}{I_p(0)\exp(-2gI_lz) - I_s(0)}.$$

Defining the depletion length as the length over which the Stokes intensity drops to $1/e$ of its maximum [i.e., $I_s(l_{dep}) = (1/e)I_s(0)$], we find

$$l_{dep} = \frac{1}{2gI_l}\ln\left(1 + \frac{I_l(e-1)}{I_p(0)}\right),$$
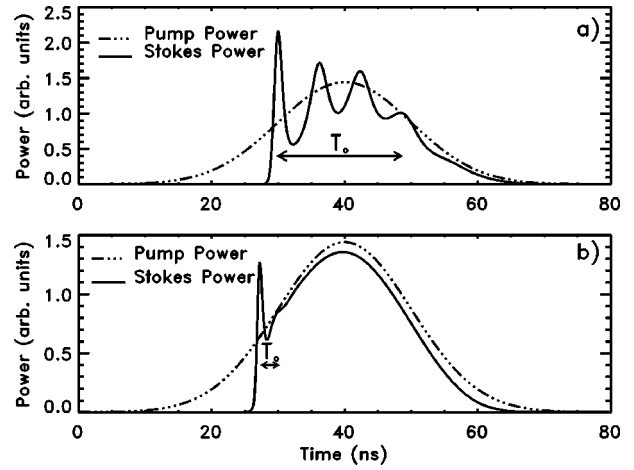
which can be approximated as

FIG. 7. Modulations present in (a) (focal length 100 cm, immersion length 40 cm) are almost suppressed in (b) (focal length 100 cm, immersion length 10 cm). Shorter immersion length provides a better suppression. Other parameters as in Fig. 3.

$$l_{dep} \approx \frac{l_{imm}}{G} \tag{10}$$

for highly depleted pump (i.e., $I_l \to 0$), and using the definition of G.

A parallel physical explanation of conditions under which temporal fluctuations are suppressed is given by Gaeta and Boyd [11]. They discuss how a spike with temporal variation $T_s = \Gamma^{-1}$ is suppressed when $G > \Gamma T_t$ (where $T_t = nl_{imm}c^{-1}$ is the transit time and $G = gI_pl_{imm}$ is the steady state gain). This condition ($G > \Gamma T_t$) is similar to the Kuzin *et al.* [21] condition (i.e., $T_{l_{dep}} < T_s$), if we use the depletion length given by Eq. (10).

Keeping constant all other parameters and varying only the immersion length, by changing the cell to lens separation, we can examine the effect of immersion length on the threshold oscillations. Figure 7 shows the behavior of the threshold oscillation for two different immersion lengths. For a smaller immersion length, Fig. 7(b), the depletion region of the pump beam is confined to a small region at the entrance of the cell resulting in a shorter relaxation oscillation.

It thus appears possible to use the advantages of a short focal length and a short immersion length to smooth out the oscillations. These conditions are confirmed to provide the best temporal fidelity of pump pulse in SBS process, Fig. 8, and appear to agree with preliminary experimental results [32]. A more complete experimental investigation is planned for a later publication.

4. Pulse compression

As mentioned previously the threshold relaxation oscillation is due to the energy interchange between the pump and the Stokes fields. We can expect to achieve pulse compression if we do not provide the appropriate amount of energy for the Stokes pulse to rebuild after the first impulse of relaxation oscillation. Figure 9 shows how the relaxation oscillation converts to a compressed pulse as input energy is reduced from (a) to (d). The process of pulse compression can be better seen if we look at the three-dimensional (3D) graph
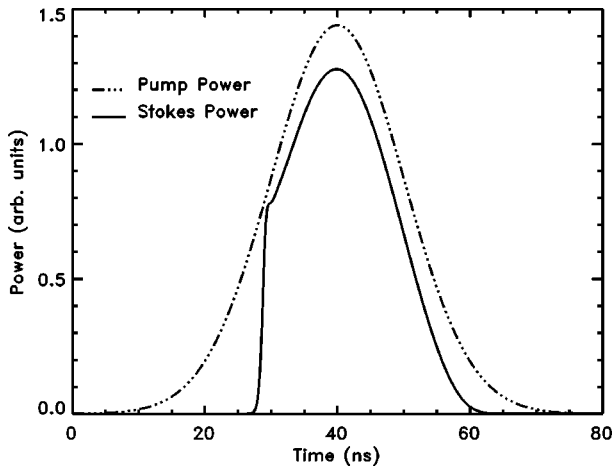
FIG. 8. Threshold oscillations disappear for short focal length and immersion length. Immersion length 20 cm and focal length 60 cm, other parameters as standard set shown in Fig. 3.

of the Stokes power, Fig. 10. At early times of the process, the center of maximum reflectivity (maximum of the Stokes pulse) is close to the focal region. This center moves towards the entrance of the cell at a later time. As a result, latter parts of the incoming pulse are traveling a shorter distance before generating the Stokes return, resulting in pulse compression [3,4].

B. Stochastic fluctuations of phase and amplitude

Noise initiation of the SBS process results in large scale fluctuations in the Stokes output. These fluctuations are of stochastic nature in the sense that there is a random probability for the occurrence of the fluctuations as well as for their temporal position in the output Stokes pulse. Corresponding and simultaneous to these fluctuations in the Stokes power, there are some rapid changes in the Stokes phase (see Fig.
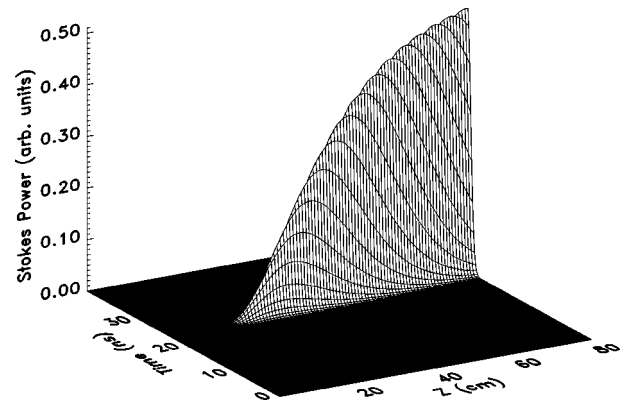

FIG. 10. 3D graph of pulse compression [(d) in Fig. 9]. Stokes power in time and space shows how the center of maximum reflectivity moves towards the entrance of the SBS cell ($z = 80$ cm) resulting in pulse compression. Parameters as in Fig. 9.

11). The simultaneous occurrence of jumps in the Stokes phase and fluctuations in the Stokes power can be understood from the main equations governing SBS [Eqs. (3)]. On the right hand side of these equations there are two effective gain terms, $g \sin(\phi_q + \phi_s - \phi_p)$ or $g \cos(\phi_q + \phi_s - \phi_p)$ which are affected by rapid changes in phase of the fields. Figure 11(b) shows how the normalized effective gain $g \sin(\phi_q + \phi_s - \phi_p)$ suffers a reduction at the time when a phase jump occurs in the Stokes field. Depending on the size of the phase jump and the phase behavior of the pump and acoustic field, the effective gain can be reduced or even become negative, which interchanges the role of Stokes and pump field, i.e., the pump field gains while the Stokes field depletes. This is similar to what happens in the generation of solitons in stimulated Raman scattering [33]. The final temporal position of phase jumps as well as the shape of the fluctuations in the output of the Stokes phase and power depend on how they propagate and amplify from the initiation point (focal
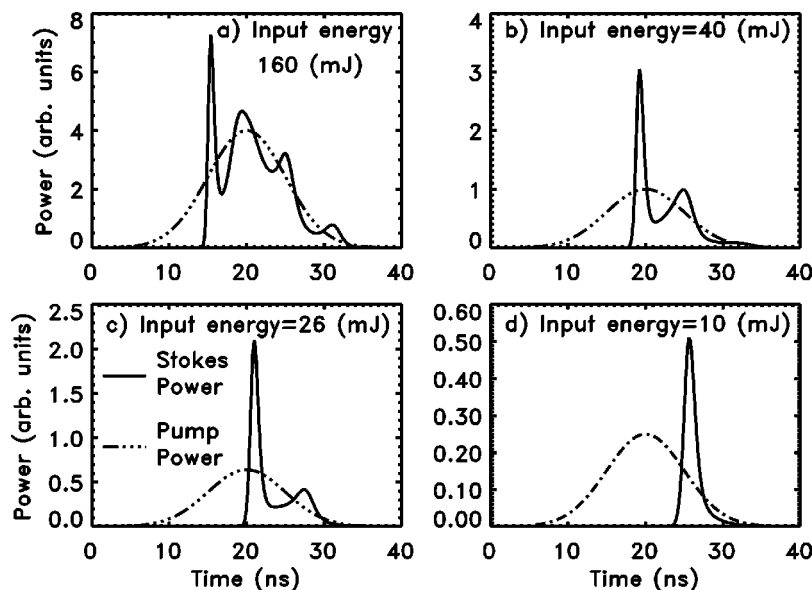

FIG. 9. Pump and Stokes power as function of time at the entrance to the cell. By reducing the pump energy, we remove extra oscillations from the threshold oscillations, resulting in a pulse-compressed beam. Cell length 80 cm, focal length 80 cm, and immersion length 70 cm with all other parameters as in Fig. 3. In (d) the delay in peak Stokes and peak pump is due to the round-trip time of the cell and building to threshold.
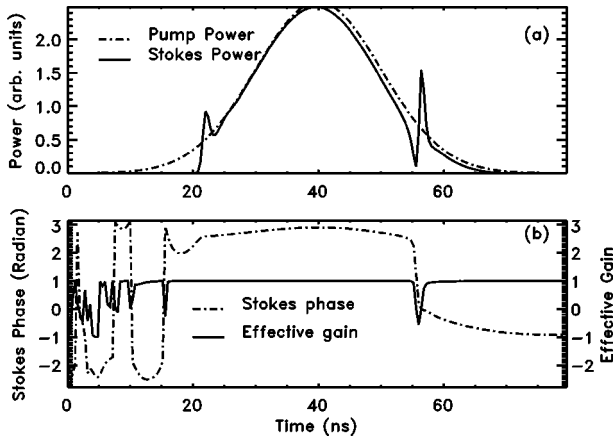
FIG. 11. Corresponding and simultaneous to each fluctuation in the Stokes output, (a), there is a jump in the Stokes phase [dashed curve in (b)]. Parameters are set as cell length 60 cm, focal length 60 cm, immersion length 30 cm, phonon lifetime 0.85 ns, gain of the medium 0.0063 cm/MW, refractive index 1.36, FWHM pulse length 20 ns, and input energy 119 mJ.

point) towards the entrance of the cell. Stokes pulses, initiated from noise, are amplified in two main regions as they propagate towards the output of the cell. In the first region, initial amplification and spectrum narrowing of the Stokes beam growing from noise take place [20,34,35,11,36,21]. The second region of length l_{dep} [Eq. (10)] is where the final amplification of the Stokes beam to a level approximately equal to the pump power occurs. The final Stokes output can be greatly affected by the dynamic processes in the depletion region. As previously discussed, this region plays a crucial role in the suppression of fluctuations in the Stokes signal when $T_{l_{dep}} < T_s$. For $T_{l_{dep}} > T_s$, however, fluctuations in the Stokes pulse experience amplification and spectrum changes, and appear in the final output [21]. It has been shown that different spectra of the fluctuations in the Stokes pulse expe-

rience different gain depending on the phonon lifetime and the length of this region [36,21]. As a result, the output spectrum of the fluctuations is different from the input when propagating through the depletion region [36,21]. Considering this and the fact that the depletion lengths l_{dep} corresponding to different temporal parts of the Stokes beam are different [see Eq. (10), where the gain $G(t) = gI_p(t)l_{imm}$ is a function of time], lead to changes in the shape of fluctuations as well as the temporal position of corresponding phase jumps in propagating through the depletion region. The results from our model also display such behavior, as shown in Fig. 12. It shows the temporal position of the phase jump and the beginning of the fluctuation in Fig. 11 as a function of time at different positions in the cell.

The focusing geometry of the SBS cell, input energy, and phonon lifetime of the material affect the phase jump fluctuations. Due to the stochastic nature of the fluctuations, the width, magnitude, and the number of fluctuations vary from pulse to pulse. As a result, we have chosen the fraction of the Stokes energy contained in the fluctuations, i.e., $\langle E_{fluc}/E_{output} \rangle$ (where $\langle \ \rangle$ means statistical average over all number of pulses) as the best parameter to show the importance of the fluctuations to a practical deployment of SBS in a laser system. Unless otherwise stated, the following parameters are applied for the numerical simulations: cell length 60 cm, focal length 60 cm, immersion length 30 cm, phonon lifetime 0.85 ns, input beam radius at window 0.3 cm, gain of the medium 0.0063 cm/MW, input energy 119 mJ, FWHM pulse length 20 ns, and refractive index 1.36.

1. Phonon lifetime effect on the phase jump fluctuations

As was previously discussed, the phonon lifetime is a measure of the acoustic field inertia. For a medium with a long phonon lifetime, the acoustic field cannot respond quickly to the rapid fluctuations in the noise initiated Stokes field, and it thus broadens and smoothens out the fluctuations in the Stokes field. To examine the effect of phonon lifetime
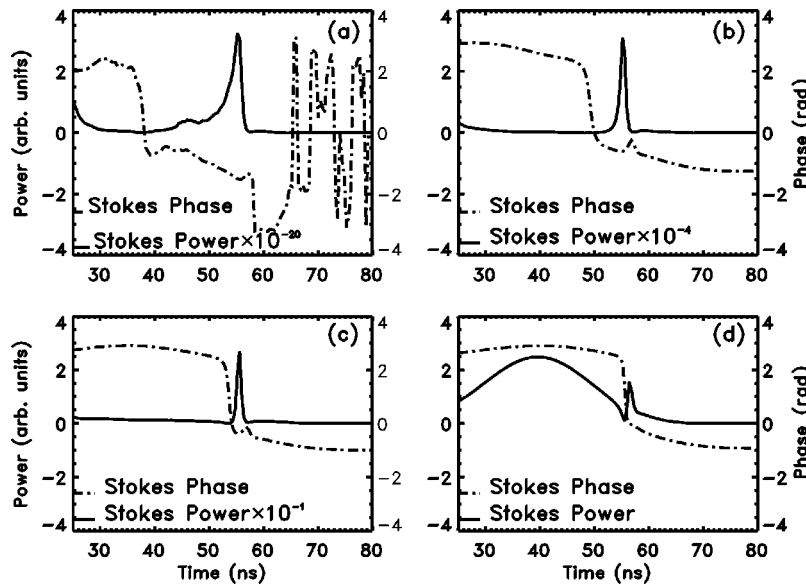

FIG. 12. The temporal position of phase jump and the beginning of the amplitude fluctuation (in Fig. 11) as they initiate at about $z = 0.46L$ (a) inside the cell (where L is the cell length) and propagate through points $z = 0.56L$ (b) and $z = 0.71L$ (c) to the entrance of the cell (d).
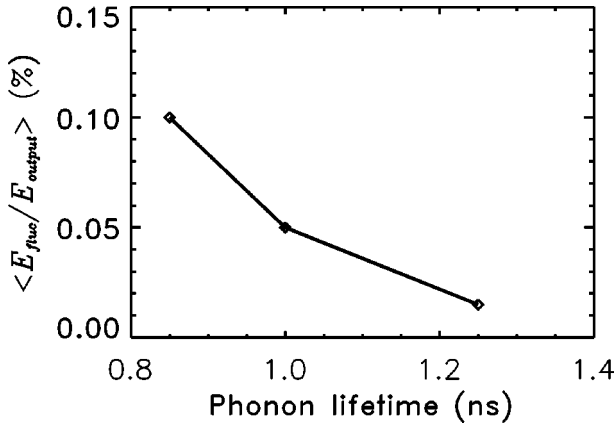
FIG. 13. Averaged fluctuation's energy (normalized to output energy) reduces for longer phonon lifetimes. Other parameters are as in Fig. 11.

on the phase jump fluctuations, the simulation model was run with different initial noise distributions for three different phonon lifetimes. The fluctuation energy (normalized to the output energy and averaged over a certain number of shots) is calculated for these different phonon lifetimes. Figure 13 shows how the energy of the fluctuations decreases for higher phonon lifetime, indicating a better suppression of fluctuations for long phonon lifetimes.

2. Effect of immersion length

As mentioned previously, the two key parameters in suppressing the fluctuations are the propagation time through the depletion region $T_{l_{dep}}$ and the temporal variation of Stokes signal T_s which reaches the depletion region. In the case when $T_{l_{dep}} < T_s$ the fluctuations in the Stokes signal are suppressed as they pass through the depletion region while in the other case, $T_{l_{dep}} > T_s$, they are magnified and appear in the final Stokes output. The depletion length l_{dep} depends (roughly) on the steady state gain G and the immersion length l_{imm} [see Eq. (10)]. By controlling G and l_{imm} we are thus able to change the length of depletion region. From the condition $T_{l_{dep}} > T_s$, it is clear that reducing $T_{l_{dep}}$ implies a
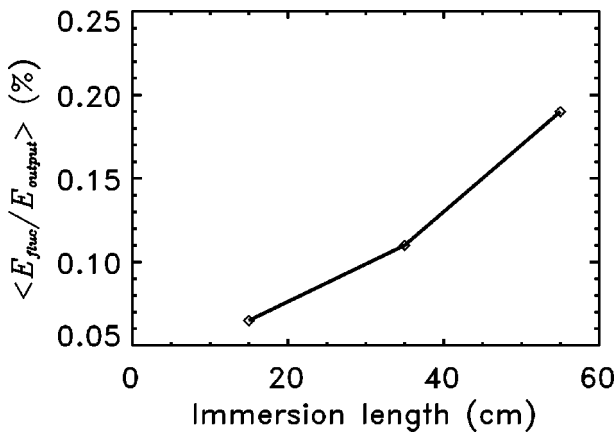

FIG. 14. The effect of the energy fluctuations, measured by $\langle E_{fluc}/E_{output} \rangle \%$, is reduced for shorter immersion lengths (constant focal length and large cell to lens separation).
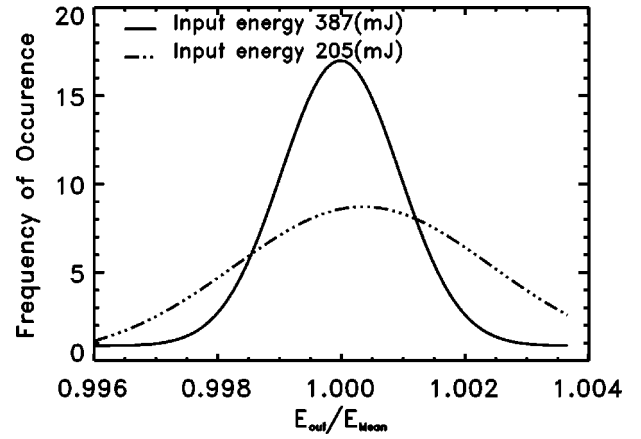

FIG. 15. Histogram of output energies (normalized to the mean) for two different energies 387 mJ and 205 mJ. Operating at high input energy reduces the effect of fluctuations.

reduction in the number of fluctuations as well as their durations in the final Stokes output.

A shorter depletion length can be obtained for a short immersion length (achieved by long cell-lens separation) and as a result, we would expect a better suppression of fluctuations. Figure 14 shows how averaged fluctuation energy $\langle E_{fluc}/E_{out} \rangle \%$ (normalized to output energy) changes as a function of the immersion length. We thus conclude that a small immersion length achieved by large cell to lens separation provides better suppression of fluctuations.

3. Effect of input energy

Another parameter that can affect the depletion length is input energy. Higher input energy results in a higher gain G, which in turn reduces the depletion length l_{dep} of the SBS. As discussed above, we thus expect that fluctuations in the output Stokes beam have smaller duration, i.e., they carry less energy. In order to examine the effect of input energy, we have studied the output Stokes beam of 500 simulated pulses with different initial noise distribution and at different energies. Considering the histogram of $E_{out}/(\bar{E}_{out})$ for these 500 pulses, where $\bar{E}_{out}$ is the mean energy of all output
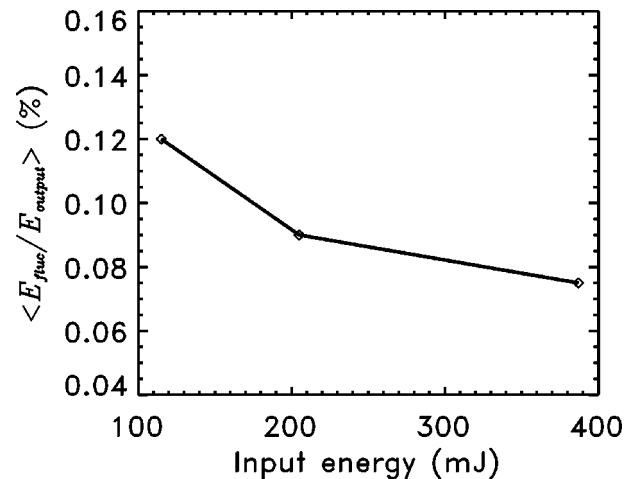

FIG. 16. A reduction in averaged fluctuation energy ($\langle E_{fluc}/E_{output} \rangle \%$) occurs at high energies.
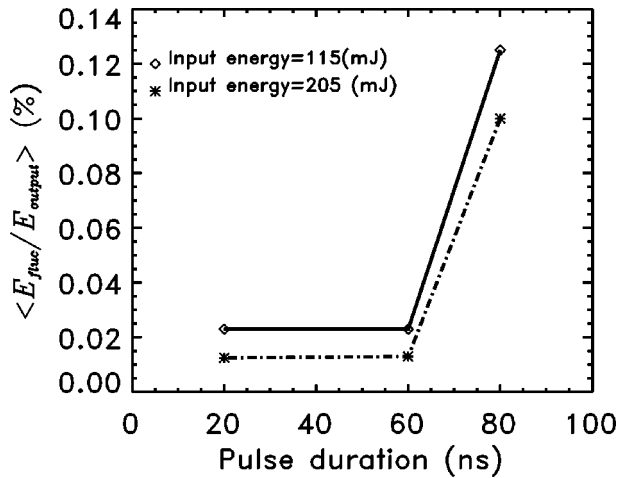
FIG. 17. For a constant energy, reducing the duration of the input pulse dramatically suppresses the fluctuation in the output Stokes. The effect of pulse duration on the suppression of fluctuations is shown for two energies: 115 mJ and 205 mJ.

pulses, and fitting a Gaussian function to it, we find that the width of the Gaussian fit is reduced at higher energy, i.e., the variation in output energy per pulse around the mean value is reduced for high energy (see Fig. 15). Another parameter that can show how fluctuations are suppressed for high energies is the average of the fluctuation energy (normalized to output energy). Simulation results in Fig. 16 show a reduction in the averaged fluctuation energy for higher input energies.

4. Effect of pulse duration

In the above section, we kept the duration of the input pulse constant and we studied the effect of parameters such as input energy and beam area on the fluctuations. In order to observe the role of pulse duration, we have chosen to keep the input energy of the pulse constant and reduced the pulse duration, i.e., we increased the peak injected power. Simulation results show a dramatic reduction in the number of fluctuations for short pulse durations which in turn results in a smaller averaged fluctuation energy (Fig. 17).

IV. CONCLUSION

To describe different kinds of temporal amplitude and phase modulations in SBS, we extended the plane-wave equations for complex fields describing SBS in a finite cell to include focusing geometry and initiation from a Gaussian random noise distributed over space and time. Two kinds of modulations were found: (1) Deterministic relaxation oscillation at the threshold energy and (2) random fluctuations in the output Stokes power.

The finite phonon lifetime of a material is responsible for an energy interchange between the pump and Stokes field resulting in relaxation oscillations at the threshold. There is no modulation of the Stokes phase corresponding to these oscillations. It is predicted that materials with shorter phonon lifetimes can exhibit relaxation oscillations of longer duration than those with long phonon lifetimes. It was found that an initially stronger acoustic wave (resulting from a high focal intensity determined by the focal length of the lens) shortens the relaxation oscillations at the threshold energy since the Stokes pulse can use the energy stored in the acoustic field after initially overshooting. Also, a small immersion length achieved by a large cell to lens separation reduces the threshold relaxation oscillations. All together, short focal length, short immersion length, and large phonon lifetime provide the best parameter space for removing the threshold relaxation oscillations.

SBS initiated from microscopic noise shows large scale stochastic amplitude modulation in the output Stokes beam. Simultaneous and corresponding jumps in the Stokes phase are observed. We have determined a parameter regime where this modulation is minimized or eliminated, thus predicting conditions for optimized, reliable SBS.

(1) Longer phonon lifetime provides a better suppression of instabilities in the Stokes pulse.

(2) Depending on the input energy and focused spot size, the pump and Stokes field can be confined to a small region near the entrance of the cell (high energies, short immersion length) or distributed towards the focal point for low energies and long immersion length. For high input energies or short immersion length the time for propagation through this region $T_{l_{dep}}$ is small enough to suppress many of the fluctuations reaching this region with duration $T_s > T_{dep}$. Short immersion length achieved by large cell to lens separation is more desirable since $T_{l_{dep}}$ can be reduced more effectively and a higher reflectivity can be achieved, but will in practice be limited by optical breakdown of the SBS material or cell window.

(3) Another parameter that can be used effectively to suppress the fluctuations is pulse duration. Our results showed that for a shorter pulse duration (i.e., higher peak power) the number of fluctuations was reduced dramatically.

[1] B. Y. Zel'dovich, N. F. Pilipetsky, and V. Shkunov, *Principles of Phase Conjugation* (Springer-Verlag, Berlin, 1985).

[2] D. A. Rockwell, IEEE J. Quantum Electron. **24**, 1124 (1988).

[3] D. T. Hon, Opt. Lett. **5**, 516 (1980).

[4] M. J. Damzen and H. Hutchinson, IEEE J. Quantum Electron. **19**, 7 (1983).

[5] N. G. Basov, V. F. Efimkov, I. G. Zubarev, A. V. Kotov, S. I. Mikhailov, and M. G. Smirnov, Pis'ma Zh. Éksp. Teor. Fiz. **28**, 215 (1978) [JETP Lett. **28**, 197 (1978)].

[6] M. Valley, G. Lombardi, and R. Aprahamian, J. Opt. Soc. Am. B **3**, 1492 (1986).

[7] K. D. Ridley and A. M. Scott, J. Opt. Soc. Am. B **13**, 900 (1996).

[8] S. M. Wandzura, in *Proceedings of the Conference on Laser and Electro-Optics, Anaheim, CA, 1988* (Optical Society of America, Washington, DC, 1988), p. 8.

[9] E. M. Dianov, A. Y. Karasik, A. V. Lutchnikov, and A. N. Pilipetskii, Opt. Quantum Electron. **21**, 381 (1989).

[10] R. W. Boyd, K. Rzazewski, and P. Narum, Phys. Rev. A **42**, 5514 (1990).

[11] A. L. Gaeta and R. W. Boyd, Phys. Rev. A **44**, 3205 (1991).

[12] T. R. Moore, A. L. Gaeta, and R. W. Boyd, in *Proceedings of International Quantum Electronics Conference, USA, 1993* (Optical Society of America, Washington, DC, 1993), pp. 394–395.

[13] M. S. Mangir, J. J. Ottusch, D. C. Jones, and A. Rockwell, Phys. Rev. Lett. **68**, 1702 (1992).

[14] W. P. Brown and S. M. Wandzura, in *Proceedings of the Conference on Laser and Electro-Optics, Anaheim, CA, 1988* (Ref. [8]), p. 10.

[15] J. Munch, R. F. Wuerker, and M. J. LeFebvre, Appl. Opt. **28**, 3099 (1989).

[16] V. Devrelis, M. O'Connor, J. Munch, S. Afshaarvahid, C. J. Wei, and A. M. Grisogono, in *Proceedings of International Quantum Electronics Conference, Sydney, Australia, 1996* (Optical Society of America, Washington, DC, 1996), p. 164.

[17] V. Devrelis, Ph.D. thesis, University of Adelaide, 1997 (unpublished).

[18] N. G. Basov, I. G. Zubarev, A. B. Miranov, S. I. Mikhailov, and A. Y. Okulov, Pis'ma Zh. Éksp. Teor. Fiz. **31**, 685 (1980) [JETP Lett. **31**, 645 (1980)].

[19] M. V. Vasil'ev, A. L. Gyulameryan, A. V. Mamaev, V. V. Ragul'skii, P. M. Semenov, and V. G. Siderovich, Pis'ma Zh. Éksp. Teor. Fiz. **31**, 673 (1980) [JETP Lett. **31**, 634 (1980)].

[20] V. I. Bespalov, A. A. Betin, G. A. Pasmanik, and A. A. Shilov, Pis'ma Zh. Éksp. Teor. Fiz. **31**, 668 (1980) [JETP Lett. **31**, 630 (1980)].

[21] E. Kuzin, M. Petrov, and A. Fotiadi, *Principles of Phase Conjugation* (Springer-Verlag, Berlin, 1994).

[22] J. C. Englund and C. M. Bowden, Phys. Rev. Lett. **57**, 2661 (1986).

[23] C. M. Bowden and J. C. Englund, Opt. Commun. **67**, 71 (1988).

[24] Y. Akiyama, K. Midorikawa, M. Obara, and H. Tashiro, J. Opt. Soc. Am. B **8**, 2459 (1991).

[25] D. C. MacPherson, R. C. Swanson, and J. L. Carlsten, Phys. Rev. Lett. **61**, 66 (1988).

[26] W. Kaiser and M. Maier, in *Stimulated Rayleigh, Brillouin and Raman Spectroscopy, Laser Handbook*, edited by F. T. Arecchi and E. O. Schuls-Dubis (North-Holland, Amsterdam, 1972), Vol. 2, pp. 1077–1149.

[27] G. C. Valley, IEEE J. Quantum Electron. **22**, 704 (1986).

[28] A. Kummrow and H. Meng, Opt. Commun. **83**, 342 (1991).

[29] R. Chu, M. Kanefsky, and J. Falk, J. Appl. Phys. **71**, 4653 (1992).

[30] R. Menzel and H. J. Eichler, Phys. Rev. A **46**, 7139 (1992).

[31] C. L. Tang, J. Appl. Phys. **37**, 2945 (1966).

[32] M. O'Conor, Ph.D. thesis, University of Adelaide, 1997 (unpublished).

[33] D. C. MacPherson and J. L. Carlsten, J. Opt. Soc. Am. B **4**, 1853 (1987).

[34] Z. M. Benenson *et al.*, Pis'ma Zh. Éksp. Teor. Fiz. **42**, 164 (1985) [JETP Lett. **42**, 202 (1985)].

[35] E. M. Dianov, A. Y. Karasik, A. V. Lutchnikov, and A. K. Senatorov, Kvant. Elektron. (Moscow) **16**, 778 (1989) [Sov. J. Quantum Electron. **19**, 508 (1989)].

[36] A. A. Fotiadi and E. A. Kuzin, in *Proceedings of International Quantum Electronics Conference, USA, 1994* (Optical Society of America, Washington, DC, 1994), p. 84.